(glass) that formed the perimeter of the basal plane. Our geometry differs from Hillig's in that each facet is bounded by both a foreign material (the cell windows) and the other facet. This geometry allows us to measure the relative growth velocity of the two facet planes. The maximum undercooling is the same for both faces. The ratio of the velocities of the two faces determines the direction of advance of their intersection. If the velocity v of each face is given by an independent nucleation process, then this ratio will be given by (*10*)

$$\frac{v_1}{v_2} \propto e^{-(\alpha_1 - \alpha_2)/\Delta T} \qquad (2)$$

where α_1 and α_2 are related to the nucleation barriers on the individual facet planes. For a homogeneous 2D nucleation process, $v_1 = v_2$, predicting a specific direction for the facet growth. For heterogeneous nucleation, $\alpha_1 \neq \alpha_2$, and as the supercooling is decreased, the velocity of one of the planes would predominate, causing the facets to move in a different, well-defined direction.

When the temperature is ramped quickly, causing the ice perimeter to advance at a high velocity, the facets grow out in a purely radial direction (Fig. 4). This is what might be expected when the growth rate of each facet is limited by the dissipation of latent heat. In the limit of slow growth, we expect the facet growth to be governed by interface processes such as 2D nucleation. On reducing the growth rate, the growth direction changes and approaches a new heading that is rate-independent. Interestingly, this direction is not the one obtained by assuming either homogeneous or heterogeneous nucleation. Consequently, we speculate that the growth process for each plane is not independent of the other, but rather is controlled in some nontrivial way by their common boundary.

The presence of the facets also provides an opportunity to study the relaxation of twist along grain boundaries. As the ice interface grows out, the grain boundary orientation at the ice edge is pinned to the line of intersection of the two basal facets. Once formed, however, a grain boundary would like to relax to an orientation that minimizes its free energy. In the absence of any anisotropy in the interfacial energies, the minimum energy orientation would be vertical (perpendicular to the plane of the ice disk) because this minimizes the grain boundary area. When anisotropy is included, the grain boundary may prefer some other orientation. In Fig. 1B, the grain boundary has relaxed from the pinned orientation at the edge to a more energetically favored one at smaller radius.

The faceted grooves observed here were not rare examples: typically, 10 to 20% of all grooves were faceted. This percentage is attributed to the cell geometry and the manner in which the ice is nucleated. Nucleation is accomplished by suddenly imposing a sharply lower temperature at the center of the top face of the cell, forcing a temperature gradient normal to the window plane. Initial growth is in the same direction, during which the fastest growing domains may wedge out other orientations. Because ice grows fastest along the *a* axis, the result is to produce domains with the *c* axis mostly in the plane of the ice disk.

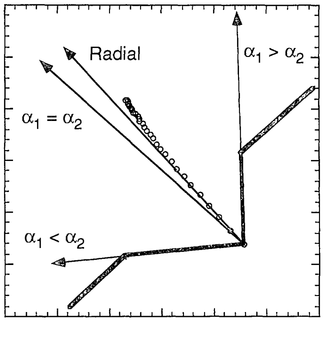

Fig. 4. The position of the vertex (circles) plotted relative to the ice-water interface (bold line) at equally spaced time intervals. The vertex initially grows out quickly in a radial direction but converges to a new direction as the growth slows. Also shown are the theoretical directions for homogeneous nucleation ($\alpha_1 = \alpha_2$) and heterogeneous nucleation ($\alpha_1 \neq \alpha_2$).

REFERENCES AND NOTES

1. C. Herring, in *The Physics of Powder Metallurgy*, W. E. Kingston, Ed. (McGraw-Hill, New York, 1951).
2. G. F. Bolling and W. A. Tiller, *J. Appl. Phys.* **31**, 1345 (1960); G. E. Nash and M. E. Glicksman, *Philos. Mag.* **24**, 577 (1971); D. R. H. Jones and G. A. Chadwick, *ibid.* **22**, 291 (1970); S. C. Hardy, *ibid.* **35**, 471 (1977); ______, G. B. Mcfadden, S. R. Coriell, P. W. Voorhees, R. F. Sekerka, *J. Cryst. Growth* **114**, 467 (1991); W. W. Mullins and P. G. Shewmon, *Acta Metall.* **7**, 163 (1959).
3. E. Arbel and J. W. Cahn, *Surf. Sci.* **66**, 14 (1977); P. W. Voorhees, S. R. Coriell, G. B. Mcfadden, R. F. Sekerka, *J. Cryst. Growth* **67**, 425 (1984).
4. L. A. Wilen and J. G. Dash, *Phys. Rev. Lett.* **74**, 5076 (1995).
5. W. K. Burton, N. Cabrera, F. C. Frank, *Philos. Trans. R. Soc. A* **243**, 299 (1951).
6. J. D. Weeks and G. H. Gilmer, *Adv. Chem. Phys.* **40**, 157 (1979).
7. Such a situation is analogous to nucleation in three dimensions; see D. Turnbull, in *Solid State Physics: Advances in Research and Applications*, F. Seitz and D. Turnbull, Eds. (Academic Press, New York, 1956), pp. 256–262.
8. W. B. Hillig, in *Growth and Perfection of Crystals*, R. H. Doremus, B. W. Roberts, D. Turnbull, Eds. (Wiley, New York, 1958), pp. 350–360.
9. A. A. Chernov, *Modern Crystallography III: Crystal Growth* (Springer, Berlin, 1984); D. P. Woodruff, *The Solid-Liquid Interface* (Cambridge Univ. Press, London, 1973); J. Taylor, J. W. Cahn, C. A. Handwerker, *Acta Metall.* **40**, 1443 (1992); A. J. Vilenkin and A. Brokman, *J. Cryst. Growth* **123**, 261 (1992); J. S. Wettlaufer, M. Jackson, M. Elbaum, *J. Phys. A* **27**, 5957 (1994); M. Adda Bedia and M. Ben Amar, *Phys. Rev. E* **51**, 1268 (1995); E. Raz, S. G. Lipson, E. Polturak, *Phys. Rev. A* **40**, 1088 (1989).
10. We have made an implicit assumption here that the prefactor multiplying the exponential is the same for growth on both faces [(*6*), p. 184]. However, our main point is that we can test the predictions of various models with the experimental technique we describe.
11. We acknowledge many fruitful discussions with J. Wettlaufer and J. Cahn. Supported under National Science Foundation grant DMR-9400637 and Office of Naval Research grant N00014-90-J-1369.

10 July 1995; accepted 13 September 1995

Partitioning of Tungsten and Molybdenum Between Metallic Liquid and Silicate Melt

Michael J. Walter* and Yves Thibault

The "excess" of siderophile elements in Earth's mantle is a long-standing problem in understanding the evolution of Earth. Determination of the partitioning behavior of tungsten and molybdenum between liquid metal and silicate melt at high pressure and temperature shows that partition coefficients ($D_{\mathrm{metal/silicate}}$) vary by two orders of magnitude depending on whether metal segregated from a basaltic or peridotitic melt. This compositional dependence is likely a response to changes in the degree of polymerization of the silicate melt caused by compositional variations of the network-modifying cations $Mg^{2+}$and Fe^{2+}. Silicate melt compositional effects on partition coefficients for siderophile elements are potentially more important than the effects of high pressure and temperature.

If core formation in the Earth was a simple equilibrium process whereby metal segregated from silicate, then the abundance of siderophile (metal-seeking) elements retained in the silicate mantle of the Earth should reflect the conditions of equilibrium. On the basis of metal/silicate partitioning data collected at 1 atm and low-temperature conditions (1600 to 1900 K) (*1*, *2*), siderophile elements are overabundant in the Earth's upper mantle by as much as several orders of magnitude (*3*). Recent numerical models of the thermal history of the early Earth that are based on large-impact accretion models (*4*) predict large or wholesale melting of the proto-Earth (*5*, *6*). If core formation occurred during this time, then segregation may have been a high-pressure and high-temperature process. It has been postulated that both pressure and temperature significantly affect siderophile element partitioning behavior (*7*, *8*). Several studies have reported liquid metal/silicate melt partitioning data at extreme pressures and temperatures (*9*–*11*) and have shown, for example, that increasing pressure and temperature significantly reduces the partitioning coefficient of liquid metal/silicate melt ($D_{met/sil}$) for Ni and Co. Element partitioning between coexisting phases potentially depends on the bulk composition of a system, but it has been assumed in previous partitioning studies and in models of core formation that the bulk composition of the silicate, with the exception of oxygen content, does not have a significant effect on metal/silicate partitioning. Here, we present results on the partitioning behavior of W and Mo—both highly charged moderately siderophile elements (W^{6+} and Mo^{6+})—between liquid metal and silicate melt as a function of silicate melt composition, temperature, and pressure.

Mixtures with bulk compositions in the system Si-Al-Fe-Mg-Ca-(W or Mo) were prepared from high-purity powdered oxides, carbonate ($CaCO_3$), and metals (Fe, W, and Mo). Iron was added to mixtures as Fe_2O_3 and Fe metal, and the oxygen content of these mixtures was varied by changing the ratio of Fe_2O_3 to Fe in the mix. In our study of Ni and Co partitioning, the relative abundances of Si, Al, Mg, and Ca were fixed at that for a model C1 chondrite (*11*). Here, we varied not only oxygen content among the starting materials, but also Si/Mg from ~0.7 to ~2.1, a range that encompasses Si/Mg of fertile peridotite (~0.9), chondrite (~1.1), komatiite (~1.2), and picritic basalt (~2.2). The value of $D_{met/sil}$ depends on experimental conditions and can be quite large for W and Mo (>1000). This makes electron microprobe analysis of their abundances in the quenched silicate impossible if chondritic abundances are used in starting mixtures [for example, 92.6 ppb of W and 928 ppb of Mo (*12*)]. For this reason, we added 10% by weight of either W or Mo to each mixture. Starting mixtures were loaded into graphite sample containers. Although carbon became an integral component of the metal alloys (~5 weight %) in our experiments, only an insignificant amount of carbon is believed to have dissolved in the silicate melt (*11*).

We report here experiments made at 2 and 6 GPa, and from 2300 to 2700 K, for the W-bearing samples, and at 1 and 7 GPa, and from 2200 to 2700 K, for the Mo-bearing samples (Table 1). Experiments were run either in a piston cylinder or multi-anvil apparatus (*13*). Our results show that for W at 2 GPa and 2300 K (Fig. 1A), log $D_{met/sil}$ varies as a function of oxygen fugacity (f_{O_2}) and Si/Mg according to the linear relation

$$\log D_{met/sil} = a + b(f_{O_2}) + c(\mathrm{Si/Mg})$$

A least-squares fit reproduces the data to within ~2% average deviation [weighted sum of deviation squared (WSDS) = 0.05]. At constant values of f_{O_2}(essentially constant FeO in the silicate), log $D_{met/sil}$ drops by more than a log unit as a result of variation in Si/Mg from 1.3 to 0.7. Thus, as the relative abundance of Mg^{2+} increases and that of Si^{4+} decreases in the silicate melt, W becomes more soluble. Similar results were obtained for Mo (Fig. 1B). Again, the solubility of Mo in the silicate melt increases as Si/Mg decreases.

Table 1. Data for experiments with W- and Mo-bearing samples. Microprobe data are available upon request. Uncertainties given in parentheses are ±2 SEM. Values for f_{O_2} were as calculated in (*21*).

Run	log D	f_{O_2} (ΔIW)	Si/Mg	NBO/T
		W, 2 GPa, 2300 K		
10	3.33(7)	−1.91(1)	1.27(1)	2.01
47	2.87(4)	−1.76(1)	1.18(2)	2.18
17	2.74(3)	−1.63(1)	1.27(1)	2.12
34	2.57(3)	−1.52(1)	1.27(3)	2.17
39	2.17(2)	−1.32(1)	1.29(2)	2.27
43	1.92(1)	−1.19(1)	1.28(4)	2.41
57*	1.99(1)	−1.31(1)	1.21(3)	2.46
08	2.00(3)	−1.45(1)	1.03(3)	2.58
20	1.73(3)	−1.28(1)	1.02(3)	2.71
12	1.53(6)	−1.20(3)	1.06(4)	2.69
54	1.57(2)	−1.64(2)	0.73(1)	3.40
55	1.32(4)	−1.40(3)	0.75(2)	3.51
56	2.16(3)	−1.71(1)	0.88(3)	2.83
58	2.53(5)	−1.93(2)	0.78(4)	3.07
59	3.5†	−1.70(1)	2.10(1)	1.30
		W, 2 GPa, 2600 K		
23	3.16(5)	−1.87(1)	1.25(1)	2.04
48	2.80(3)	−1.74(2)	1.17(4)	2.19
18	2.67(2)	−1.56(1)	1.25(1)	2.16
37	2.48(2)	−1.51(1)	1.29(3)	2.10
40	2.18(2)	−1.34(1)	1.25(1)	2.34
44	1.95(1)	−1.20(1)	1.27(1)	2.43
		W, 6 GPa, 2300 K		
01	3.5†	−2.13(2)	1.21(2)	2.05
28	2.95(5)	−1.78(2)	1.20(1)	2.17
49	2.84(5)	−1.77(1)	1.16(3)	2.21
38	2.57(3)	−1.53(1)	1.23(1)	2.24
41	2.12(3)	−1.34(2)	1.24(1)	2.36
42	2.08(3)	−1.24(1)	1.29(1)	2.40
		W, 6 GPa, 2700 K		
51	2.93(3)	−1.83(1)	1.17(2)	2.16
50	2.65(2)	−1.75(2)	1.14(1)	2.25
46	2.11(1)	−1.40(1)	1.14(2)	2.50
		Mo, 1 GPa, 2200 K		
01	3.64(7)	−1.47(1)	1.10(2)	2.35
07	3.41(8)	−1.22(2)	1.11(4)	2.53
12	3.02(14)	−1.01(4)	1.11(5)	2.71
15	3.06(10)	−1.62(1)	0.74(2)	3.33
16	2.65(7)	−1.24(4)	0.77(2)	3.55
		Mo, 1 GPa, 2600 K		
03	3.26(7)	−1.48(2)	1.09(1)	2.44
09	3.03(10)	−1.31(3)	1.11(1)	2.49
13	2.79(13)	−1.08(5)	1.07(7)	2.73
		Mo, 7 GPa, 2300 K		
02	3.34(10)	−1.50(1)	1.10(1)	2.40
05	3.07(8)	−1.25(2)	1.11(1)	2.50
11	2.73(10)	−1.08(3)	1.10(2)	2.67
		Mo, 7 GPa, 2700 K		
04	2.90(2)	−1.43(1)	1.12(1)	2.39
10	2.46(4)	−1.25(3)	1.13(1)	2.49
14	2.35(7)	−1.04(4)	1.11(2)	2.72

*Experiment with only 5% W in the starting material. †W below detection limit. $D_{mel/sil}$ is a minimum.

At constant Si/Mg, the only composi-

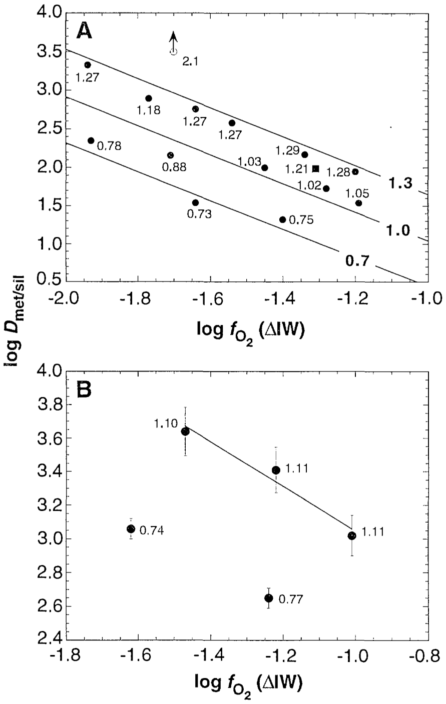

Fig. 1. Log $D_{met/sil}$ versus log f_{O_2} (ΔIW) for W at 2 GPa and 2300 K (**A**). Values for $D_{met/sil}$ are in weight percent. Analytical uncertainties are about the size of the symbols for W. Individual data points are labeled according to the Si/Mg of the silicate melt. Linear contours of constant Si/Mg (solid lines) were calculated by best-fit multiple linear regression to all the solid circular data points with the equation $\log D = a + b(\log f_{O_2})$ (ΔIW) + c(Si/Mg) (WSDS = 0.05). The slope of the regressed contours is −1.9. The open circle, not included in the regression, is from an experiment in which W was below the detection limit, so its partition coefficient is shown as a lower bound. The solid square is from an experiment with only 5% W rather than the usual 10%. (**B**) Mo data at 1 GPa and 2200 K. Numbers are as in (A). Error bars show analytical uncertainty (2 SEM). The regressed slope to data with constant Si/Mg of ~1.1 has a slope of −1.3 (r^2 = 0.96).

M. J. Walter, Geophysical Laboratory and Center for High Pressure Research, Carnegie Institution of Washington, 5251 Broad Branch Road NW, Washington, DC 20015, USA.

Y. Thibault, Department of Earth Sciences, Biology and Geology Building, University of Western Ontario, London, Ontario N6A 5B7, Canada.

*To whom correspondence should be addressed at Institute for Study of Earth's Interior, Okayama University, Misasa, Tottori-ken 682-01, Japan.

tional parameter that varies in the bulk composition is oxygen, producing variations of FeO in the silicate melt from ~8 weight % at 2 log units below the iron-wustite buffer (IW-2) to ~20 weight % at IW-1. The equilibrium equation describing the partitioning of W or Mo between metal and silicate can be written as

$$M^{met} + (y/2)O_2 = MO_y^{sil}$$

where *M* is the metal cation and *y* is determined by the valence state of the cation in the silicate. In a solution in which the metal species in the silicate and metallic liquids mix ideally, the valence state of *M* in the silicate is given by a linear relation between log $D_{met/sil}$ and log f_{O_2} such that

$$\log D_{met/sil} = A \cdot \log f_{O_2} + B$$

where $A = -y/2$, and *B* contains activity and equilibrium constant terms that are assumed to be constant at constant temperature and pressure (*2*). If W exists in the silicate melt in a 6^+ valence state, then the slope of the lines of constant Si/Mg (where only FeO of the silicate melt varies) on Fig. 1A should be −1.5. The observed slope is −1.9, however, and this value yields a calculated valence of 7.6, which is impossible for W. Our results at 6 GPa and 2300 K yielded a valence of 6.6, again larger than the ideal value of 6. The apparent increase in valence could be an artifact of a systematic change in the activity of iron in the silicate with changing values of f_{O_2}. A recent experimental study by Hillgren (*14*) was designed to test this hypothesis, and for values of f_{O_2} in the range of IW-1 to IW-2, Hillgren's results showed a constant difference between calculated and measured values of f_{O_2}.

Thus, on the basis of these results, no change in slope on Fig. 1 would be expected as a result of changing activity of FeO in the silicate. One possible explanation is that the nonideal slope for W reflects changes in the solution behavior of the W species in the silicate melt with changing Fe^{2+} in the melt. This presumption is supported by the decrease in log $D_{met/sil}$ associated with decreasing Si/Mg of the silicate melt (that is, increasing Mg^{2+}). The slope of log $D_{met/sil}$ versus that of log f_{O_2} for Mo (Fig. 1B) yielded a valence of 5.2, and data at 7 GPa yielded a valence of 5.6. However, uncertainties in $D_{met/sil}$ are larger for Mo than for W, and we have fewer data, so we cannot resolve the meaning of this value.

What compositional parameters produce our observed increase in W and Mo solubility in the silicate melt will depend on the molecular species present in the silicate melts produced here. A qualitative model can be constructed to describe the observed behavior. The SiO_4 tetrahedra are the basic structural units in silicate melts and, depending on how oxygen atoms are shared with neighboring tetrahedra (bridging oxygens), they form a variety of possible network structures (*15*). Intensive variables such as composition, temperature, and pressure can have systematic effects on melt speciation—for example, the type and abundance of structural units such as SiO_4^{4-}, $Si_2O_5^{2-}$, and $Si_2O_7^{6-}$. Cations that are not tetrahedrally coordinated, such as Mg^{2+} and Fe^{2+}, must compete for oxygen atoms in the melt structure (nonbridging oxygens), and in doing so they depolymerize the melt structure and create new opportunities for competition for oxygen by cationic species. Highly charged cations such as W and Mo have a strong affinity for oxygen, and their solution properties may be influenced by silicate structure (*16*). On the basis of available data, highly charged cations should be most strongly partitioned into depolymerized silicate melts (*17*).

Here, we calculated the number of nonbridging oxygens to tetrahedrally coordinated cations (NBO/T) for the silicate melts in our experiments (Table 1). NBO/T gives the degree of polymerization of a silicate melt, with a value of 0 indicating a fully polymerized melt and a value of 4 indicating a completely depolymerized melt (*15*). The silicate melts have calculated NBO/T values ranging from ~1.3 to 3.6. We fit partitioning data for W at 2 GPa and 2300 K to a linear equation of the following form:

$$\log D_{met/sil} = a + b(f_{O_2}) + c(\mathrm{NBO/T})$$

A least-squares regression reproduced the data to within ~3% average deviation (weighted sum of deviation squared = 0.06). If NBO/T is a reasonable proxy for the complex variables in the silicate melt that cause the observed changes in W and Mo solubility, then changes in log $D_{met/sil}$ as a function of log f_{O_2} should not be affected at constant NBO/T. The calculated valence of W at constant NBO/T is ~5.8 (compare to a valence of 7.6 calculated from the slope at constant Si/Mg on Fig. 1A), a value that is close to the ideal valence of 6^+. This near ideal calculated valence likely reflects the compositional dependence of W solubility on the abundance of network-modifying cations such as Fe^{2+} and Mg^{2+}. Hillgren *et al.* (*18*) have also obtained experimental evidence that shows a dependence of $D_{met/sil}$ for W and Mo on silicate melt composition. Their data suggest that other siderophile and lithophile elements (Ni, Co, P, Ga, and Ge) are also affected, although the magnitude of these effects has yet to be isolated.

Support for the importance of melt structure on partitioning comes from a study on the effect of pressure on albite melt structure made by Keppler and Rubie (*19*). They showed that an increase in pressure in the range of 5 to 10 GPa increases the opportunities for octahedral coordination of Ni and Co, thereby making them more soluble in the melt. Since that study, it has been confirmed that Ni and Co become more soluble in melts of basaltic to peridotitic composition with increase in pressure and temperature (*9*–*11*), and this phenomenon likely reflects a change in silicate melt structure. On the basis of our data over a range of temperatures and pressures (Table 1), at constant silicate melt composition $D_{met/sil}$ for W shows no change, within uncertainty, with increase in temperature or pressure. However, log $D_{met/sil}$ for Mo decreases at a rate of ~0.07 per 1 GPa, and 0.1 per 100 K, over the range of conditions we investigated.

A possible reason for changes in the W and Mo solubility in the silicate melts in our experiments is extreme deviation from behavior according to Henry's law. We feel that this is not a primary effect for the following reasons. The liquid metal alloy phase contains ~30 weight % of W or Mo, so it is likely that activity-composition relations do not follow Henry's law at such high concentrations. However, the variation in W and Mo in the liquid metals among experiments with different bulk compositions is typically about 2 to 5%, and these changes should not produce such large changes in W and Mo solubility in the silicate. The silicate melts contain between 100 ppm and 15,000 ppm of W (most have <10,000 ppm) and between 100 and 2000 ppm of Mo.

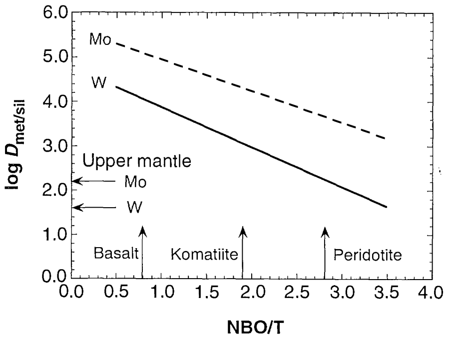

Fig. 2. Log $D_{met/sil}$ for W (solid line) and Mo (dashed line) as a function of NBO/T at log f_{O_2} (ΔIW) of −1.9. The trends are extrapolations based on linear regressions to the W data at 2 GPa and 2300 K [excluding runs W57 and W59 (Table 1)], and to the Mo data at 1 GPa and 2200 K, according to the equation log $D = a + b \log f_{O_2}$ (ΔIW) + c(NBO/T) (WSDS = 0.06 for W and 0.01 for Mo). Also shown are the NBO/T of typical tholeiitic basalt, komatiite, and peridotite compositions, and the log $D_{met/sil}$ that is necessary to account for the abundances of W and Mo in the upper mantle assuming equilibrium core formation between an Fe-rich core making up ~30% of the mass of Earth.

To test the effect of W concentration in the coexisting metal and silicate phases on partitioning, we used only 5% by weight of W in the bulk composition at 2 GPa and 2300 K (Fig. 1A, solid square). Within uncertainty, our result was consistent with data obtained with the usual 10% of W in the bulk composition. This result suggests that deviations from Henry's law cannot account for the observed effect of silicate melt composition on partitioning. At constant values of f_{O_2}, temperature, pressure, and W concentration in the bulk composition, variations in Si/Mg from 1.3 to 0.7 produced nearly an order of magnitude change in values of $D_{met/sil}$, whereas changing the W concentration by half produced no observable change in partitioning.

Segregation of metal from silicate to form Earth's core almost certainly involved both a liquid metal and a silicate melt, although the amount of silicate melt necessary to promote metal segregation could be small (*20*). Depending on the degree of melting, the silicate melt in equilibrium with metal could range essentially from basalt (low melt fraction) to peridotite (high melt fraction). For a value of f_{O_2} at which core segregation will leave a mantle with ~9% FeO by weight, $D_{met/sil}$ for W is $\sim10^4$, and for Mo is $\sim10^5$, in a melt of basaltic composition (Fig. 2). However, in a peridotitic melt, $D_{met/sil}$ for W and Mo drops to $\sim10^2$ and $\sim10^3$, respectively. Thus, depending on the degree of melting of the mantle in the Earth's early history, W and Mo partition coefficients can vary over two orders of magnitude. When the added effects of temperature and pressure on Mo partitioning are taken into account (for example, increasing pressure by 5 GPa and temperature by 500 K decreases the value of D for Mo by about 1 log unit) the magnitude of the abundances of W and Mo in the upper mantle can be explained by equilibrium between liquid-metal and ultra-mafic silicate melt at high pressures and temperatures (Fig. 2). This result gives support to models that show the core segregating from a highly or completely molten early Earth.

REFERENCES AND NOTES

1. J. H. Jones and M. J. Drake, *Nature* **322**, 221 (1986).
2. W. Schmitt, H. Palme, H. Wänke, *Geochim. Cosmochim. Acta* **53**, 173 (1989).
3. H. E. Newsom, in *Origin of the Earth*, H. E. Newsom and J. H. Jones, Eds. (Oxford Univ. Press, New York, 1990), pp. 273–288.
4. G. W. Wetherill, *Science* **228**, 877 (1985).
5. H. J. Melosh, in *Origin of the Earth*, H. E. Newsom and J. H. Jones, Eds. (Oxford Univ. Press, New York, 1990), pp. 69–84.
6. W. Benz and A. G. W. Cameron, *ibid.*, pp. 61–68.
7. A. E. Ringwood, *Proc. R. Soc. London* **A395**, 1 (1984).
8. V. R. Murthy, *Science* **253**, 303 (1991).
9. D. Walker, L. Norby, J. H. Jones, *ibid.* **262**, 1858 (1993).
10. V. J. Hillgren, M. J. Drake, D. C. Rubie, *ibid.* **264**, 1442 (1994).
11. Y. Thibault and M. J. Walter, *Geochim. Cosmochim. Acta* **59**, 991 (1995).
12. E. Anders and N. Grevesse, *ibid.* **53**, 197 (1989).
13. Talc-Pyrex cells were used in piston-cylinder experiments and, on the basis of a calibration of known phase transitions, pressure is accurate to ±0.05 GPa. MgO-cast octahedral cells were used in multi-anvil experiments. On the basis of a high-temperature (1500 K) pressure calibration of known phase transitions, and with the use of WC second-stage anvils with 11-mm truncated edge lengths, pressure uncertainty was ±0.4 GPa. Graphite resistance heaters were used to produce temperatures from 2200 to 2700 K, and temperature was measured with type D (W/Re) thermocouples. Temperature uncertainties were estimated at ±15 K in piston-cylinder experiments, and ±30 K in multi-anvil experiments. Experiments were held at temperature between 300 and 600 s in all experiments, which was sufficient time for equilibrium between silicate melt and liquid metal at the experimental temperatures (*11*). Runs were quenched by shutting off power to the furnace. Run products consisted of quenched liquid metal spheres that segregated during the experiment and quenched silicate melt composed of fine- to coarse-grained intergrowths of crystallites. We analyzed run products with an electron microprobe using a 15-kV accelerating potential and a 30- and 100-nA beam current for metal and silicate, respectively. Probe areas ranged from 10 to 50 μm², and acquisition times were 30 and 120 s for major and trace elements, respectively.
14. V. J. Hillgren, *Proc. Lunar Planet. Sci. Conf.* **26**, 607 (1995).
15. B. O. Mysen, *Structure and Properties of Silicate Melts* (Elsevier, Amsterdam, 1988).
16. P. C. Hess, in *Physical Chemistry of Magmas*, L. L. Perchuk and I. Kushiro, Eds. (Springer-Verlag, New York, 1991), pp. 152–191.
17. A. J. Ellison and P. C. Hess, *Eos* **70**, 487 (1989).
18. V. J. Hillgren, M. J. Drake, D. C. Rubie, unpublished results.
19. H. Keppler and D. C. Rubie, *Nature* **364**, 54 (1993).
20. D. J. Stevenson, in *Origin of the Earth*, H. E. Newsom and J. H. Jones, Eds. (Oxford Univ. Press, New York, 1990), pp. 231–250.
21. M. J. Drake, H. Newsom, S. J. B. Reed, M. C. Enright, *Geochim. Cosmochim. Acta* **53**, 2101 (1989). Iron variations in the silicate melt are inextricably linked to variations in f_{O_2} according to the IW buffer reaction

$$\mathrm{Fe}_{\mathrm{metal}} + \frac{1}{2}\mathrm{O}_2 = \mathrm{FeO}_{\mathrm{silicate}}$$

If ideal behavior is assumed, a value of f_{O_2} can be calculated relative to the IW buffer reaction simply from the mole fractions of Fe and FeO in the metal and silicate. See also (*10*), where

$$\log f_{O_2}\,(\Delta\mathrm{IW}) = 2.0 \log \frac{X^{\mathrm{sil}}_{\mathrm{FeO}}}{X^{\mathrm{met}}_{\mathrm{Fe}}}$$

22. We thank M. Drake, T. Duffy, Y. Fei, M. Humayin, V. Kress, B. Mysen, and an anonymous reviewer for helpful comments and reviews of the manuscript, and V. Hillgren for a preprint and a helpful discussion. We also thank K. Hadidiacos for invaluable assistance with the microprobe. M.J.W. acknowledges support from the Geophysical Laboratory and Center for High Pressure Research, Carnegie Institution of Washington.

10 July 1995; accepted 5 September 1995

Fas Ligand–Induced Apoptosis as a Mechanism of Immune Privilege

Thomas S. Griffith, Thomas Brunner, Sharon M. Fletcher,
Douglas R. Green, Thomas A. Ferguson*

The eye is a privileged site that cannot tolerate destructive inflammatory responses. Inflammatory cells entering the anterior chamber of the eye in response to viral infection underwent apoptosis that was dependent on Fas (CD95)–Fas ligand (FasL) and produced no tissue damage. In contrast, viral infection in *gld* mice, which lack functional FasL, resulted in an inflammation and invasion of ocular tissue without apoptosis. Fas-positive but not Fas-negative tumor cells were killed by apoptosis when placed within isolated anterior segments of the eyes of normal but not FasL-negative mice. FasL messenger RNA and protein were detectable in the eye. Thus, Fas-FasL interactions appear to be an important mechanism for the maintenance of immune privilege.

That some sites in the body are immunologically "privileged" has been recognized for more than 120 years (*1*). Classically, an immune-privileged site is where allogeneic or xenogeneic (*2, 3*) tissue grafts enjoy prolonged survival relative to other areas. Thus, these sites have been defined as regions in the body where the immune system appears not to function. One example of such a site is the eye, where even minor episodes of inflammation can result in impaired vision or even blindness if the inflammation proceeds unchecked. The concept of immune privilege in the eye has been extended to include infectious organisms and tumor cells (*4, 5*), because placing these into immune-privileged sites does not elicit destructive or protective immunity. Although several explanations

T. S. Griffith and S. M. Fletcher, Department of Ophthalmology and Visual Sciences, Washington University School of Medicine, St. Louis, MO 63110, USA.
T. Brunner and D. R. Green, Division of Cellular Immunology, La Jolla Institute for Allergy and Immunology, La Jolla, CA 92037, USA.
T. A. Ferguson, Departments of Ophthalmology and Visual Sciences and Pathology, Washington University School of Medicine, St. Louis, MO 63110, USA.

---

*To whom correspondence should be addressed.